Molecular beam epitaxy of metamorphic $In_yGa_{1-y}P$ solar cells on mixed anion $GaAs_xP_{1-x}$/GaAs graded buffers

Stephanie Tomasulo,[a] John Simon, Paul J. Simmonds,
Jonathan Biagiotti, and Minjoo L. Lee
Department of Electrical Engineering, Yale University, P.O. Box 208284, New Haven, Connecticut 06520-8284

(Received 27 October 2010; accepted 8 December 2010; published 7 March 2011)

The authors have grown metamorphic $In_yGa_{1-y}P$ on optimized $GaAs_xP_{1-x}$/GaAs graded buffers via solid source molecular beam epitaxy (MBE) for multijunction solar cell applications. In this work, the authors show that a previously developed kinetic growth model can be used to predict the composition of mixed anion $GaAs_xP_{1-x}$ alloys on GaAs as a function of substrate temperature and group-V flux. The advantages of using a high growth temperature of 700 °C are then described, including the minimized dependence of composition on small temperature variations, a linear dependence of film composition on incident group-V flux ratio, and the ability to attain low threading dislocation densities of $\leq 10^6$ cm^{-2}. The authors then discuss the effect of faceted trenches, a morphological defect specific to tensile strain relaxation, on minority carrier properties, as well as strategies to eliminate them. Growth temperature effects, phase separation, and difficulties encountered in *n*-type doping of InAlP:Si are then described in the context of $In_yGa_{1-y}P$ solar cell growth. The MBE growth techniques presented here have enabled the demonstration of 2.00 eV band gap metamorphic $In_{0.39}Ga_{0.61}P$ solar cells, exhibiting open-circuit voltages as high as 1.42 V. These results indicate that metamorphic $In_yGa_{1-y}P$ is a promising material for future multijunction solar cells. © *2011 American Vacuum Society.* [DOI: 10.1116/1.3559119]

I. INTRODUCTION

Metamorphic triple-junction solar cells have recently reached efficiencies of 41.1% by combining lattice-mismatched light-absorbing materials, each efficiently collecting a different portion of the solar spectrum.[1] Calculations show that four to six junction cells could approach efficiencies of 60%, but these cell designs will require top subcells with band gap (E_g) energies ranging from 2.0 to 2.2 eV.[2–4] Most III-V materials available in this range possess indirect band gaps, necessitating thick absorber layers to fully collect the incoming sunlight. Furthermore, many of these materials contain Al, whose affinity for oxygen leads to efficiency-diminishing defects.[5–8]

$In_yGa_{1-y}P$ ($y=0.27-0.40$), in contrast, has a direct band gap in the desired range and is Al-free. It is, however, lattice-mismatched to conventional substrates. In order to grow lattice-mismatched $In_yGa_{1-y}P$ films with low threading dislocation densities (TDDs) and long minority carrier lifetimes, we employ an intermediate $GaAs_xP_{1-x}$ graded buffer to engineer the lattice constant from that of GaAs to that of wide-E_g $In_yGa_{1-y}P$. $GaAs_xP_{1-x}$ graded buffers grown by both metalorganic chemical vapor deposition[9,10] (MOCVD) and molecular beam epitaxy[11] (MBE) have recently been demonstrated. However, the unequal and temperature-dependent incorporation rates of the anionic species create challenges in achieving reproducible composition control.

In this work we first show that a kinetic growth model, previously used to describe anion incorporation in gas-source MBE of $GaAs_xP_{1-x}$, can be extended to solid source MBE (SSMBE) of $GaAs_xP_{1-x}$.[12] We then discuss the growth of each component of a single junction wide-E_g $In_yGa_{1-y}P$ solar cell individually, including the graded buffer, $In_yGa_{1-y}P$ active region, and InAlP window layer. Taken together, the growth techniques described in this paper have recently led to the demonstration of high open-circuit voltage (V_{oc}) metamorphic $In_yGa_{1-y}P$ solar cells.

II. EXPERIMENT

All samples were grown on GaAs (100) substrates in a Veeco GEN-II SSMBE chamber equipped with *in situ* reflection high energy electron diffraction (RHEED), allowing surface monitoring during growth. Our system contains elemental sources of Ga, In, Al, Be, Si, P, and As, with thermal cracking of the group-V species performed at 900 °C to produce dimer beam fluxes. All fluxes reported here are beam equivalent pressures (BEPs) while substrate temperatures (T_{sub}) refer to thermocouple readings; thermocouple temperatures of 650 and 700 °C were found to correspond to approximate pyrometer temperatures of 645 and 680 °C, respectively. After growth, we determined material composition and degree of relaxation using x-ray diffraction (XRD) measurements on a Bede-D1 system with a Cu K_α source, while Nomarski optical microscopy allowed us to characterize surface morphologies. We carried out photoluminescence (PL) measurements using a 527 nm laser and an Ocean Optics USB 2000 spectrometer to estimate material band gaps and to confirm compositions acquired via XRD. We performed both cross-sectional-view (XV) and planar-view (PV) transmission electron microscopy (TEM) on a Tecnai

[a]Electronic mail: stephanie.tomasulo@yale.edu

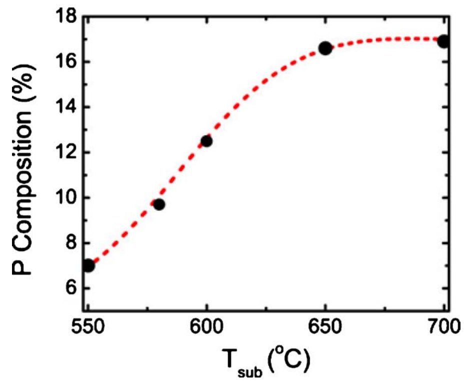

FIG. 1. (Color online) P composition of $GaAs_xP_{1-x}$ samples grown under identical $P_2/(As_2+P_2)$ flux ratio at various values of T_{sub} (●). Fit (- - -) with model from Ref. 12. The composition dependence of $GaAs_xP_{1-x}$ on T_{sub} is minimized between 650 and 700 °C.

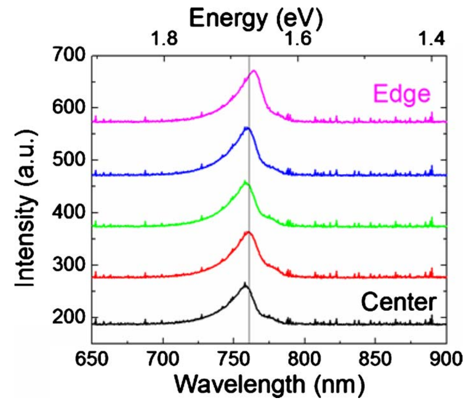

FIG. 2. (Color online) Room temperature PL spectra of a $GaAs_{0.8}P_{0.2}$ graded buffer collected from various positions on a 4 in. wafer. PL emission wavelength remains nearly constant from center to edge of the $GaAs_{0.8}P_{0.2}$ graded buffer, indicating minimal T_{sub}-dependent composition variation at T_{sub} =700 °C.

T12 system operated at 120 kV to inspect interfaces and to determine TDDs, respectively. High angle annular dark field (HAADF) imaging, performed in a Tecnai Osiris scanning TEM operated at 200 kV, was used to complement the results from conventional TEM imaging. To calibrate the doping necessary for solar cell structures, we grew thick (~1–2 μm) test samples with different dopant fluxes and measured carrier concentrations using a van der Pauw Hall effect system with a 0.51 T magnet. A 15–20 nm heavily doped GaAs cap layer was found to facilitate Ohmic contact formation, particularly for Al-containing samples. Using In solder contact points as a hard mask, the GaAs cap was selectively etched away to avoid errors resulting from parallel conduction in the GaAs cap layer. We fabricated single junction $In_yGa_{1-y}P$ solar cells and measured lighted current-voltage (L-IV) characteristics using a Newport solar simulator with a Keithley 2400 source meter.

III. RESULTS AND DISCUSSION

A. $GaAs_xP_{1-x}$ graded buffers on GaAs

We grew a series of $GaAs_xP_{1-x}$ buffers at T_{sub} =550–700 °C while keeping the $P_2/(As_2+P_2)$ flux constant in order to measure the kinetics of anion incorporation; the V/III BEP ratio was ~20. XRD confirmed that T_{sub}-dependent composition variation can be minimized between 650 and 700 °C, as previously observed in Ref. 12 (Fig. 1). Using simple kinetic models, Liang and Tu[12] found that $GaAs_xP_{1-x}$ composition varies as a function of T_{sub} as $x=1/[1+C(f_{As_2}/f_{P_2})]$, where f_{As_2} and f_{P_2} are the As_2 and P_2 fluxes, respectively, and C is given by

$$C=\frac{2.7\{1+X\exp[-21\,500/T_{sub}](1+B)\}}{1+Y\exp[-29\,250/T_{sub}](1+A)}, \tag{1}$$

where A and B are

$$A=Z\exp(-15\,000/T_{sub}), \tag{2}$$

$$B=K\exp(-18\,000/T_{sub}). \tag{3}$$

By adjusting the pre-exponential terms (X, Y, Z, and K) in Eqs. (1)–(3) and using beam equivalent pressures to obtain $f_{As_2}/f_{P_2}=7$, we fit our data using $X=7.5\times10^{10}$, $Y=2.5\times10^{15}$, $Z=3.5\times10^{6}$, and $K=4.4\times10^{8}$ (Fig. 1).

PL measurements, taken across a graded $GaAs_xP_{1-x}$ buffer grown at T_{sub}=700 °C on a 4 in. semi-insulating GaAs wafer, further confirmed the minimized T_{sub}-dependent composition variation predicted in the model of Liang and Tu.[12] The results demonstrated a peak wavelength variation from center to edge of ±3 nm, yielding an As composition (assuming similar degrees of relaxation) variation of <1% (Fig. 2).

In addition to improved composition control, another advantage of using high T_{sub} for $GaAs_xP_{1-x}$ growth is that the desorption rates of P and As become nearly equal for T_{sub} ≥650 °C.[12] Thus, P incorporation versus P_2 flux transitions from a superlinear dependence for T_{sub}≤580 °C to a simple linear dependence for T_{sub}≥650 °C. Employing a step-graded structure, we controlled the composition of each layer in the $GaAs_xP_{1-x}$ graded buffers by varying the P_2 flux in a stepwise fashion while keeping the As_2 flux constant [Fig. 3(a)], which led to uniform changes in phosphorous content from step to step. Figure 3(b) shows that P composition is linearly dependent on the $P_2/(As_2+P_2)$ flux ratio at T_{sub} =700 °C, again confirming the kinetic model of Liang and Tu.[12]

The dislocation dynamics model of Fitzgerald *et al.* shows that a further benefit of growing at high T_{sub} is improved kinetics for dislocation glide, which, in turn, should lead to lower TDD.[13] In agreement with this model, our PVTEM measurements revealed that growing $GaAs_{0.8}P_{0.2}$ at T_{sub}=700 °C resulted in TDD=$(0.7-1.0)\times10^6$ cm^{-3}, while growing at T_{sub}=650 °C resulted in TDD=$(2.0-3.0)\times10^6$ cm^{-3} (Fig. 4). Thus, lower TDD, a linear composition dependence on P flux, and minimized composition dependence on T_{sub} are all enabled by growing at T_{sub}≥650 °C.

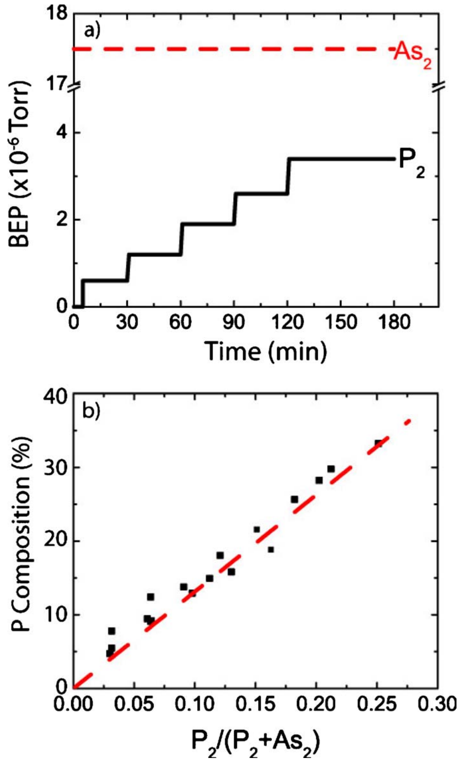

FIG. 3. (Color online) (a) Control of composition changes during mixed anion $GaAs_xP_{1-x}$ graded buffer growth. P_2 flux (—) is stepped to change the composition of each layer in the buffer while keeping As_2 flux (- - -) constant. (b) Samples grown under various $P_2/(As_2+P_2)$ flux ratios (■) show that composition varies linearly with $P_2/(As_2+P_2)$ flux ratio at 700 °C (- - - is linear fit to data).

At $T_{sub} \geq 650$ °C, the Ga adatom sticking coefficient can no longer be assumed to be unity, and thus the growth rate will be decreased compared with growth at lower T_{sub}.[14] We recalibrated the growth rate for elevated T_{sub} by growing a GaAs film at $T_{sub}=700$ °C with a Ga flux known to provide a growth rate of 920 nm/h for $T_{sub}=580$ °C (where the Ga sticking coefficient is close to unity). By growing the GaAs film between two AlGaAs marker layers, we were able to measure the resulting GaAs thickness using cross-sectional scanning electron microscopy (XSEM). We then found the GaAs growth rate at $T_{sub}=700$ °C to be 700 nm/h, 25% lower than the growth rate at $T_{sub}=580$ °C. This growth rate

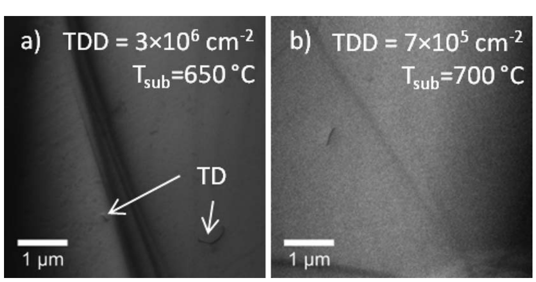

FIG. 4. PVTEM of $GaAs_{0.8}P_{0.2}$ graded buffers grown at T_{sub} equal to (a) 650 °C and (b) 700 °C. Reduced TDD is observed at $T_{sub}=700$ °C.

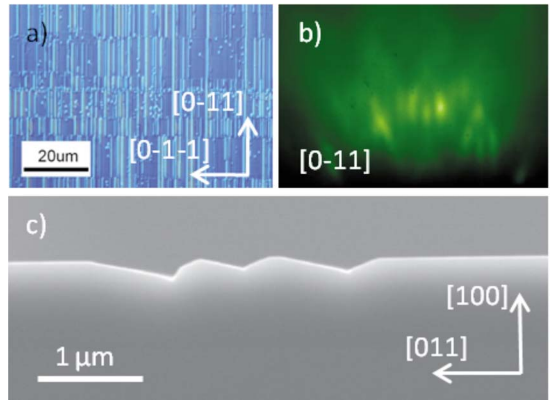

FIG. 5. (Color online) (a) Nomarski micrograph of FTs (streaks on surface) with a density of 528 cm^{-1}. (b) RHEED pattern along $[0\bar{1}1]$ shows chevrons as a result of high-FTD. (c) XSEM of FTs reveals a depth of 100–300 nm.

reduction should thus be taken into account when growing graded buffers at high T_{sub} in order to avoid an unintentional increase of the grading rate.

We observed that unoptimized $GaAs_xP_{1-x}$ graded buffer structures suffered from a morphological defect propagating along the $[0\bar{1}1]$ direction, which we refer to as a faceted trench (FT).[11] Using Nomarski microscopy we calculated FT densities (FTDs) by adding the lengths of each of the FTs and dividing by the measured area, yielding a value with units of cm^{-1} [Fig. 5(a)]. A FTD exceeding 500 cm^{-1} is observable *in situ* as a streaky chevron-like RHEED pattern along $[0\bar{1}1]$ [Fig. 5(b)]. The orientation of the FT planes can be determined from the angle the chevron makes with the vertical streak. In this way we obtained a facet angle of 24°–29° (verified by XSEM), which implies that the trenches form facets on the {113}*A* or {114}*A* planes. Using XSEM we also measured the depth of the FTs to be ~100–300 nm [Fig. 5(c)]. Similar morphologies, with facets only forming parallel to $[0\bar{1}1]$, have also been observed in other tensile-strained systems.[15–17]

While FTs alone may not compromise device performance, PVTEM analysis of high-FTD $GaAs_xP_{1-x}$ graded buffers revealed that FTs hinder dislocation glide and lead to threading dislocation (TD) pileups.[11] The nucleation of additional TDs is then required to relieve any remaining strain, leading to higher global TDD.[18] To investigate the effect of FTs on the electronic properties of the material, we inspected a 2.0 V forward-biased $In_{0.39}Ga_{0.61}P$ solar cell (described in Sec. III D) containing a single FT [Fig. 6(a)] under an optical microscope. The electroluminescence image in Fig. 6(b) shows that FTs locally quench radiative recombination and suggests that FTs must be completely eliminated to attain high-efficiency solar cells.

In earlier work, we showed that the FTD was highly sensitive to the details of the graded buffer structure.[11] For example, by reducing the grading rate from 0.53 to 0.29% μm^{-1}, we decreased the FTD from 120 to <1 cm^{-1} for $GaAs_{0.8}P_{0.2}$ graded buffers. The resulting graded buffer

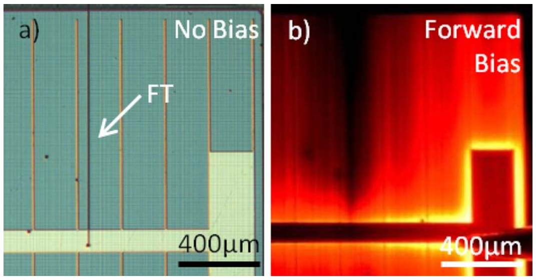

FIG. 6. (Color online) $In_{0.39}Ga_{0.61}P$ solar cell under (a) zero bias with faceted trench running down image. (b) 2.0 V forward bias. Dark regions around the FT demonstrate the ability of these defects to quench radiative recombination.

yields a high degree of strain relaxation of ~90%, measured using (400) and (422) XRD reciprocal space maps. Figure 7 provides a schematic of the graded buffer structure used in this work, which consists of nine 250-nm-thick grading steps and a 1-μm-thick cap. The P content changes by 2% for each step and terminates in a $GaAs_{0.8}P_{0.2}$ cap, resulting in a grading rate of ~0.29% μm^{-1}. In comparison, MOCVD-grown $GaAs_xP_{1-x}$ graded buffers have used similar grading rates, ranging from 0.15 to 0.20% μm^{-1},[9,10] though FTDs were not reported. It should also be noted that conditions in the MBE chamber such as growth rate and V/III BEP ratio had little effect on FTD. Optimized $GaAs_{0.8}P_{0.2}/GaAs$ graded buffers with low FTD and TDD were then used for the growth of metamorphic wide-E_g $In_yGa_{1-y}P$ solar cells.

B. Metamorphic $In_yGa_{1-y}P$ growth

To determine the optimal value of T_{sub} for $In_yGa_{1-y}P$ growth, we grew a series of $In_{0.49}Ga_{0.51}P$ films, lattice-matched to GaAs, with T_{sub}=450–490 °C. $In_{0.49}Ga_{0.51}P$ grown at 460 °C exhibited the most intense PL spectra of all samples and was therefore chosen for subsequent device growth. Although the variation in PL intensity for samples grown between 450 and 460 °C was on the order of 5%, we note that the samples grown above 470 °C exhibited ≥ ten times lower intensity than those at 460 °C.

We then grew metamorphic $In_yGa_{1-y}P$ on the optimized $GaAs_xP_{1-x}$ graded buffers described above, lattice matched

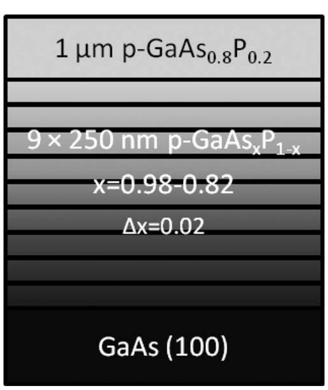

FIG. 7. Schematic of optimized $GaAs_{0.8}P_{0.2}$ graded buffer to allow metamorphic $In_{0.39}Ga_{0.61}P$ growth on GaAs.

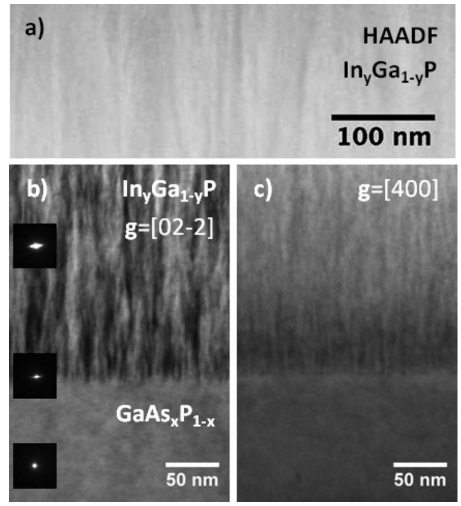

FIG. 8. (a) XVHAADF microscope image of $In_yGa_{1-y}P$. Dark regions correspond to Ga-rich domains, while light regions correspond to In-rich domains. (b) XVTEM image looking down the ⟨011⟩ zone reveals strong phase separation contrast when $\boldsymbol{g}=[02\bar{2}]$. Insets show the $(02\bar{2})$ diffraction spots taken at the $In_yGa_{1-y}P$, $In_yGa_{1-y}P/GaAs_xP_{1-x}$ interface, and $GaAs_xP_{1-x}$ film. (c) XVTEM image shows muted phase separation contrast when $\boldsymbol{g}=[400]$.

to the in-plane lattice constant of the $GaAs_{0.8}P_{0.2}$ cap as measured by XRD. We paused the growth after the graded buffer by shuttering the Ga cell and lowered T_{sub} to 460 °C under the same As_2 and P_2 overpressures used for the graded buffer cap growth. We then closed the As_2 for 1 min prior to $In_yGa_{1-y}P$ growth to minimize any As intermixing with the $In_yGa_{1-y}P$ film. The kinetic modeling results discussed in Sec. III A show that the surface likely becomes As rich during the drop in T_{sub}. However, the RHEED pattern remained streaky throughout the 20 min pause, implying that little surface roughening took place. We then grew $In_yGa_{1-y}P$ with a V/III BEP ratio of 12 at a growth rate of 0.5 $\mu m/h$.

HAADF microscopy revealed phase separation within the $In_yGa_{1-y}P$ layers. The on-pole HAADF image shows alternating dark and light contrasts along the $[0\bar{1}1]$ direction corresponding to Ga-rich and In-rich regions, respectively [Fig. 8(a)]. This striation is also clearly seen in XVTEM with a two beam condition of $\boldsymbol{g}=[02\bar{2}]$ due to the composition modulation and associated strain field in this direction [Fig. 8(b)]. However, under a two beam condition of $\boldsymbol{g}=[400]$, where the displacement field resulting from the lateral composition modulation is minimized, phase separation contrast is nearly extinguished [Fig. 8(c)]. Selected area diffraction (SAD) spots were seen to elongate into streaks along $[0\bar{1}1]$ when diffracting through phase-separated $In_yGa_{1-y}P$. The insets of Fig. 8(b) are the $(02\bar{2})$ SAD spots corresponding to the material on which they are superimposed and show the progression of diffraction spot shape from the $GaAs_xP_{1-x}$ buffer with no phase separation to the phase-separated $In_yGa_{1-y}P$. A qualitatively similar diffraction pattern was observed in phase-separated $In_{0.52}Al_{0.48}As$ where electron diffraction streaks were found to extend along [110], lateral to the growth direction.[19] Lateral composition modulation has also been observed in $In_{0.28}Ga_{0.72}P$ (Ref. 20) and other III-V alloys,[21,22] but its effect on solar cell performance remains unclear. We speculate that V_{oc} will be degraded by the In-rich lower-E_g domains, and we intend to investigate strategies to minimize phase separation in the future.

C. InAlP growth

High efficiency $In_{0.49}Ga_{0.51}P$ solar cells generally require the use of a thin $In_{0.5}Al_{0.5}P$ window layer to attain high quantum efficiencies at photon energies much larger than the E_g.[23] Typically, the window layer is grown with carrier concentration in the 10^{18} cm^{-3} range to maintain low series resistance and to minimize the extent of the depletion region resulting from the Fermi level pinning at the surface.[24] While smooth $In_{0.5}Al_{0.5}P$ layers lattice-matched to GaAs with streaky RHEED patterns could be readily grown under the same conditions used for $In_{0.49}Ga_{0.51}P$ growth, we found it difficult to obtain $In_{0.5}Al_{0.5}P$ with electron concentration $(n)>4\times10^{17}$ cm^{-3}. For example, Si/III flux ratios that would lead to $n=1\times10^{18}$ cm^{-3} in $In_{0.49}Ga_{0.51}P$ gave $n=1\times10^{17}$ cm^{-3} for $In_{0.5}Al_{0.5}P$ growth, indicating strong compensation. Significant compensation in Si-doped $(Al_{0.7}Ga_{0.3})_{0.52}In_{0.48}P$ grown by SSMBE was reported by Sun *et al.*, though they were able to reach a peak electron concentration of $n=2.1\times10^{18}$ cm^{-3}.[25] In contrast, $n=5\times10^{18}$ cm^{-3} has been reported for Si-doped $In_{0.5}Al_{0.5}P$ grown by gas-source MBE.[26,27]

In order to gain further insight on the electron compensation mechanism, we annealed our Si-doped $In_{0.5}Al_{0.5}P$, capped with a thin GaAs layer, in the MBE chamber at 680 °C for 5 min with an As_2 overpressure. Comparison with unannealed samples revealed a two to three times increase in electron concentration in the annealed $In_{0.5}Al_{0.5}P$ with a peak of $n\sim8\times10^{17}$ cm^{-3}. Several potential causes for autocompensation of group IV dopants in III-V (A-B) materials have been studied, including Si atoms on group-V sites (Si_B) instead of group III sites, nearest neighbor pairs of a Si atom on a group III site and a Si atom on a group-V site (Si_A-Si_B), and Si atoms next to group III vacancies ($Si-V_A$).[28–30] We hypothesize that one of the defect complexes present in our $In_{0.5}Al_{0.5}P$ is $Si-V_A$ and that thermal annealing gives Si atoms sufficient thermal energy to move and annihilate the group III vacancy.

D. Single junction $In_yGa_{1-y}P$ solar cells

We grew metamorphic $In_{0.39}Ga_{0.61}P$ solar cells on graded $GaAs_{0.8}P_{0.2}/GaAs$ in order to investigate the photovoltaic properties of our material. The active region of each solar cell consisted of a 2 μm p-type base, Be doped with a hole concentration of 1×10^{17} cm^{-3}, followed by a 100 nm emitter, Si doped to $n=1\times10^{18}$ cm^{-3}. The InAlP window layer was grown while increasing the Si cell temperature from 1200 °C (for emitter growth) to 1250 °C (for contact layer growth). Based upon calibration data, the window doping should be graded from $n=(1-4)\times10^{17}$ cm^{-3}. To avoid a growth interruption between the emitter and window layers, the same In flux was maintained for both $In_yGa_{1-y}P$ and InAlP growth. Bertness *et al.* used an $In_{0.53}Al_{0.47}P$ window layer with $n=4\times10^{17}$ cm^{-3} in early high-efficiency dual junction $In_{0.52}Ga_{0.48}P/GaAs$ tandem solar cells, motivating our decision to continue with a relatively low-doped window layer.[31] For contact layer growth, we grew 2 nm of GaAs at $T_{sub}=460$ °C to protect the underlying InAlP during the subsequent growth interruption, then raised T_{sub} to 580 °C to grow the remaining 50 nm of the $n=5\times10^{18}$ cm^{-3} Si-doped GaAs contact layer. A schematic of the final metamorphic $In_{0.39}Ga_{0.61}P$ solar cell structure is given in Fig. 9(a). In addition to the metamorphic $In_{0.39}Ga_{0.61}P$ cell, we grew a control $In_{0.49}Ga_{0.51}P$ cell lattice-matched to GaAs, with E_g (measured by PL) of 2.00 and 1.89 eV, respectively. The cells were processed "as grown" and were not subjected to the high-T annealing step described in Sec. III C.

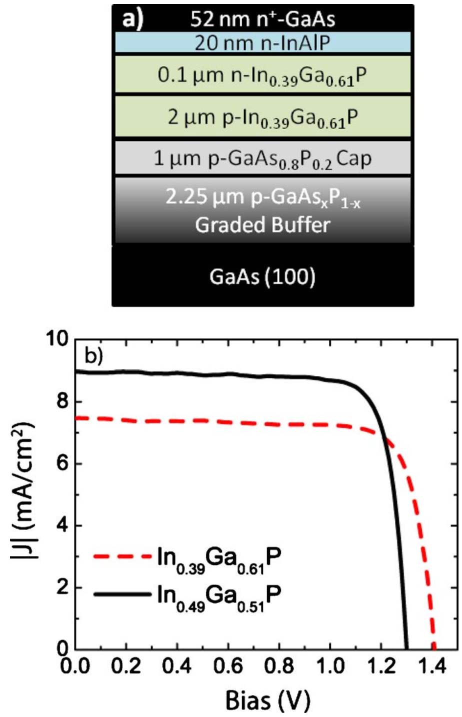

FIG. 9. (Color online) (a) Schematic of metamorphic $In_{0.39}Ga_{0.61}P$ solar cell structure. (b) L-IV curves for both $In_{0.49}Ga_{0.51}P$ (—) and $In_{0.39}Ga_{0.61}P$ (- - -) cells. V_{oc} increases with increasing E_g.

We then fabricated 2.1×2.1 mm^2 cells which were free of FTs due to the optimized grading procedure described in Sec. III A. Under approximate AM1.5G illumination conditions, we measured an increase in V_{oc} and a decrease in short circuit current for decreasing In content, consistent with expected trends for increasing E_g. The lattice-matched $In_{0.49}Ga_{0.51}P$ cell with $E_g=1.89$ eV had $V_{oc}=1.31$ V [Fig. 9(b)]. Increasing the band gap by 0.11 to 2.00 eV in the metamorphic $In_{0.39}Ga_{0.61}P$ cell led to a proportional increase of V_{oc} to 1.42 V [Fig. 9(b)]. Fill factors for both cells were nearly constant at ~0.8. The maximum practical value for V_{oc} in a 2.00 eV solar cell is ~1.60 V ($V_{oc,max}\approx E_g/q-0.40$ V).[32] By adding a back surface field and antireflective coating we aim to improve our cell performance and move closer to this maximum value of $V_{oc}=1.60$ V.

IV. SUMMARY AND CONCLUSIONS

We have demonstrated the growth of graded $GaAs_xP_{1-x}$ buffers on GaAs by SSMBE. Buffer growth at $T_{sub}=700$ °C was shown to simplify composition control and lead to low TDD. Despite the observation of significant phase separation within the $In_yGa_{1-y}P$ and difficulties in *n*-type doping of InAlP, we grew metamorphic $In_yGa_{1-y}P$ on the relaxed $GaAs_xP_{1-x}$ buffers and fabricated $E_g=2.00$ eV solar cells with $V_{oc}=1.42$ V. In future studies, the effects of phase separation and postgrowth thermal annealing will be further analyzed with the goal of identifying which defects ultimately limit V_{oc} in these devices.

ACKNOWLEDGMENTS

The authors gratefully acknowledge funding from the NSF CAREER program (Grant No. DMR-0955916). The authors also thank Dr. Jan Ringnalda for performing HAADF imaging. This research was supported in part by an award from the Department of Energy (DOE), Office of Science Graduate Fellowship Program (SCGF). The DOE SCGF Program was made possible in part by the American Recovery and Reinvestment Act of 2009. The DOE SCGF program is administered by the Oak Ridge Institute for Science and Education for the DOE. ORISE is managed by Oak Ridge Associated Universities (ORAU) under DOE Contract No. DE-AC05-06OR23100. All opinions expressed in this paper are the author's and do not necessarily reflect the policies and views of DOE, ORAU, or ORISE.

[1]W. Guter *et al.*, Appl. Phys. Lett. **94**, 223504 (2009).
[2]D. C. Law *et al.*, Sol. Energy Mater. Sol. Cells **94**, 1314 (2010).
[3]I. Tobías and A. Luque, Prog. Photovoltaics. **10**, 323 (2002).
[4]D. J. Aiken, A. B. Cornfeld, M. A. Stan, and P. R. Sharps, *IEEE 4th Conference on Photovoltaic Energy Conversion* (IEEE, New York, 2006), p. 838.
[5]C. Amano, K. Ando, and M. Yamaguchi, J. Appl. Phys. **63**, 2853 (1988).
[6]C. T. Foxon, J. B. Clegg, K. Woodbridge, D. Hilton, P. Dawson, and P. Blood, J. Vac. Sci. Technol. B **3**, 703 (1985).
[7]T. Achtnich, G. Burri, and M. Ilegems, J. Vac. Sci. Technol. A **7**, 2537 (1989).
[8]Y. Yazawa, T. Kitatani, J. Minemura, K. Tamura, K. Mochizuki, and T. Warabisako, Sol. Energy Mater. Sol. Cells **35**, 39 (1994).
[9]M. J. Mori, S. T. Boles, and E. A. Fitzgerald, J. Vac. Sci. Technol. A **28**, 182 (2010).
[10]M. A. Steiner *et al.*, *Proceedings of the 35th IEEE Photovoltaic Specialists Conference* (IEEE, New York, 2010), p. 002111.
[11]J. Simon, S. Tomasulo, P. Simmonds, M. Romero, and M. L. Lee, J. Appl. Phys. **109**, 013708 (2011).
[12]B. W. Liang and C. W. Tu, J. Appl. Phys. **74**, 255 (1993).
[13]E. A. Fitzgerald, A. Y. Kim, M. T. Currie, T. A. Langdo, G. Taraschi, and M. T. Bulsara, Mater. Sci. Eng., B **67**, 53 (1999).
[14]R. Fischer, J. Klem, T. J. Drummond, R. E. Thorne, W. Kopp, H. Morkoc, and A. Y. Cho, J. Appl. Phys. **54**, 2508 (1983).
[15]F. Cléton, B. Sieber, A. Lefebvre, A. Bensaada, R. A. Masut, J. M. Bonard, J. D. Ganière, and M. Ambri, J. Appl. Phys. **80**, 827 (1996).
[16]G. Wagner and P. Paufler, Phys. Status Solidi A **138**, 389 (1993).
[17]A. Ponchet, A. Le Corre, A. Godefroy, S. Salaün, and A. Poudoulec, J. Cryst. Growth **153**, 71 (1995).
[18]M. L. Lee, D. A. Antoniadis, and E. A. Fitzgerald, Thin Solid Films **508**, 136 (2006).
[19]S. W. Jun, T. Y. Seong, J. H. Lee, and B. Lee, Appl. Phys. Lett. **68**, 3443 (1996).
[20]M. J. Mori and E. A. Fitzgerald, J. Appl. Phys. **105**, 013107 (2009).
[21]T. S. Kuan, T. F. Kuech, W. I. Wang, and E. L. Wilkie, Phys. Rev. Lett. **54**, 201 (1985).
[22]D. Doppalapudi, S. N. Basu, K. F. Ludwig, Jr., and T. D. Moustakas, J. Appl. Phys. **84**, 1389 (1998).
[23]T. Takamoto, E. Ikeda, H. Kurita, and M. Ohmori, Sol. Energy Mater. Sol. Cells **35**, 25 (1994).
[24]J. M. Woodall and H. J. Hovel, Appl. Phys. Lett. **21**, 379 (1972).
[25]Z. Z. Sun, S. F. Yoon, and W. K. Loke, J. Cryst. Growth **235**, 8 (2002).
[26]W. Li, J. Lammasniemi, A. B. Kazantsev, R. Jaakkola, T. Makela, and M. Pessa, Electron. Lett. **34**, 406 (1998).
[27]Y. Gu, Y. G. Zhang, H. Li, A. Z. Li, and C. Zhu, Mater. Sci. Eng., B **131**, 49 (2006).
[28]E. F. Schubert, *Doping in III-V Semiconductors* (Cambridge University Press, Cambridge, 1993).
[29]J. Maguire, R. Murray, R. C. Newman, R. B. Beall, and J. J. Harris, Appl. Phys. Lett. **50**, 516 (1987).
[30]C. Domke, Ph. Ebert, M. Heinrich, and K. Urban, Phys. Rev. B **54**, 10288 (1996).
[31]K. A. Bertness, S. R. Kurtz, D. J. Friedman, A. E. Kibbler, C. Kramer, and J. M. Olson, Appl. Phys. Lett. **65**, 989 (1994).
[32]R. R. King, D. C. Law, K. M. Edmondson, C. M. Fetzer, G. S. Kinsey, H. Yoon, R. A. Sherif, and N. H. Karam, Appl. Phys. Lett. **90**, 183516 (2007).